OPTOELECTRONICS AND ADVANCED MATERIALS – RAPID COMMUNICATIONS Vol. 9, No. 9-10, September – October 2015, p. 1171 - 1175

Structural, morphological and electrical properties of heat treated $CaHPO_4$ biomaterials

IMTIAZ U. KHAWAJA[*,a], QURSHIA CHOUDHRY[b], ASIF MAHMOOD[c], ZAHEER ABAS GILANI[d], SHAUKAT ALI SHAHID[e], MUHAMMAD FAROOQ[a]

[a]*Department of Physics and Astronomy, Hazara University Mansehra-21300, Pakistan*
[b]*Department of Chemistry, The Islamia University of Bahawalpur, Bahawalpur-63100, Pakistan*
[c]*College of Engineering, Department of Chemical Engineerig, King Saud University, Riyadh, Saudi Arabia*
[d]*Department of Physics, Balochistan University of Information Technology, Engineering and Management Sciences, Quetta-87300, Pakistan*
[e]Department of Physics, University of Agriculture, Faisalabad 38040, Pakistan.

Di-calcium phosphate dihydrate triclinic $CaHPO_4.2H_2O$ was heated at 750 ^oC and 450 ^oC to obtain the tetragonal β-$Ca_2P_2O_7$ and grey-coloured tetragonal γ-$Ca_2P_2O_7$ phase. The pellets of β-$Ca_2P_2O_7$ γ-$Ca_2P_2O_7$ were prepared and dried at 120 ^oC for 4 hours. The pellets having mean thickness of 2 mm were characterized by XRD, optical microscopy, FTIR, TGA, SEM, UV-visible spectroscopy and dc-electrical measurements. Before sintering micro-cracks were seen however these cracks were disappeared after sintering at 750 ^oC. XRD confirmed the single crystalline phase. UV-vis. Spectra showed absorption in UV-region. DC-electrical resistivity exhibited that β-$Ca_2P_2O_7$ is more conducting as compared to γ-$Ca_2P_2O_7$ phase.

(Received July 7, 2015; accepted September 9, 2015)

Keywords: $CaHPO_4.2H_2O$, β-$Ca_2P_2O_7$ phase, γ-$Ca_2P_2O_7$ phase, DC-electrical resistivity, XRD, FTIR

1. Introduction

Calcium Phosphate based bio-ceramics are one of the most important materials in biomedical engineering research. There are several forms of calcium phosphate structures which normally form a family of compounds called apatite [1].These are used in the field of medical physics and medicine for the treatment of trauma and tissue defects. Hydroxyapatite (HA), a calcium phosphate compound with a chemical formula of ($Ca_{10}(PO_4)_6(OH)_2$,HA) possesses, beta tri-calcium phosphate (β-TCP, $Ca_3(PO_4)_2$ and alpha tricalcium phosphate (α-TCP, $Ca_3(PO_4)_2$ are some of the common bioactive calcium phosphate materials [2]. Calcium phosphate is one of the most common synthetic biomaterials. Calcium Phosphate based material including Hydroxyapatite having similar composition and crystal structure as that of a living bone has excellent osteoconductive and bioactive properties which could induce bone formation. Calcium phosphate ceramics such as hydrooxyapatite ($Ca_{10}(PO_4)_6(OH)_2$,HA), tri-calcium phosphate $Ca_3(PO_4)_2$, Calcium pyrophosphate ($Ca_2P_2O_7$) have good biocompatibility with human bone tissue and have been widely used as bone graft materials [3].

Hydroxyapatite is the major mineral component of human bones. From the point of view of its chemistry, it is calcium orthophosphate which has in its structure hydroxyl groups and in its stoichiometric is described with formula–$(Ca_{10}(PO_4)_6(OH)_2$ [4]. Biological properties of hydroxyapatite are very favorable; it is not only biocompatible but also bioactive. These properties made hydroxyapatite an excellent material for production of ceramic materials intended for use as implants in dentistry and treatment of orthopedic injuries [5].

Recently, CP bioceramics such as calcium phosphate, tri-calcium phosphate and HAP are identified as most suitable bone substitution materials to serve the demand. Unlike other CPs, HAp does not break under physiological conditions [6]. In fact, it is thermodynamically stable at physiological pH and actively takes part in bone bonding. This property has been exploited for rapid bone repair after major trauma or surgery. HAp is derived from natural materials such as coral and fish bone, fish scale [7]. $Ca_2P_2O_7$ is capable of interacting with surrounding bones and provide direct attachment of the implants to bone without an interposed fibrous tissue layer. This is facilitated by the presence of free calcium and phosphate compound at the surface [8]. Because of its advantages like increased tolerance of surgical inaccuracies, fast fixation of implants in bone and firm implant bone attachment has gained highly interest of the medical community in recent years [9].

2. Experimental work

2.1 Flow chart for the experimental scheme

The scheme of experimental work is depicted in the following flow chart diagram.

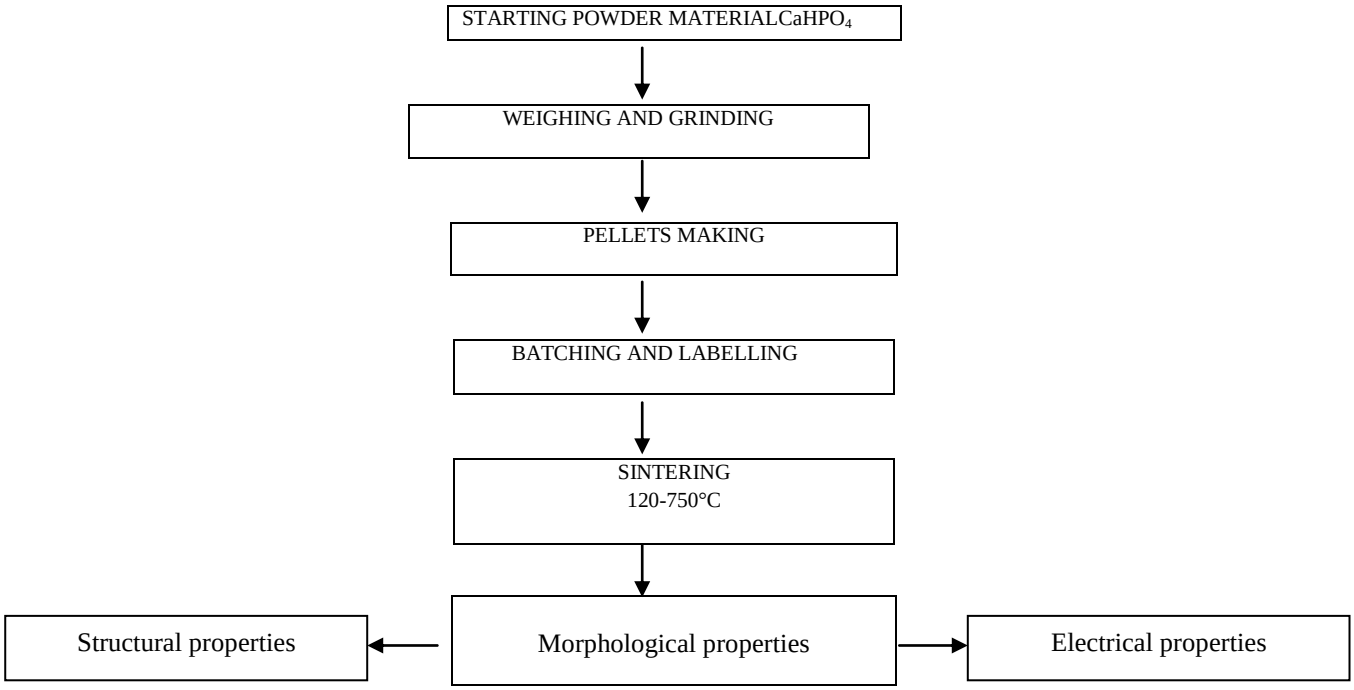

The analytical grade Di-calcium Phosphate dihydrate $2CaHPO_4.2H_2O$ (Merck, 99.9% pure) were sintered at 120 ^{o} C for removal of moisture contents. The materials were grinded by agate morter and pestal and the pellets were prepared. Then annealing at 450 ^{o} C and 750^{o} C respectively was carried for different time interval such as 6 h, 12 h, 18 h and 24hrs. The samples were characterized by XRD, SEM, TGA, UV-Visible, FTIR and dc-electrical measurements. Formation of Beta (**β**) and gamma(**γ**) phases from the precursor material can be represented by a series of chemical reactions as shown below.

$$2CaHPO_4.2H_2O \xrightarrow{120^{o}C} 2CaHPO_4 - 4H_2O \xrightarrow{450^{o}C} \gamma Ca_2P_2O_7 - H_2O \xrightarrow{750^{o}C} \beta Ca_2P_2O_7 \quad (1)$$

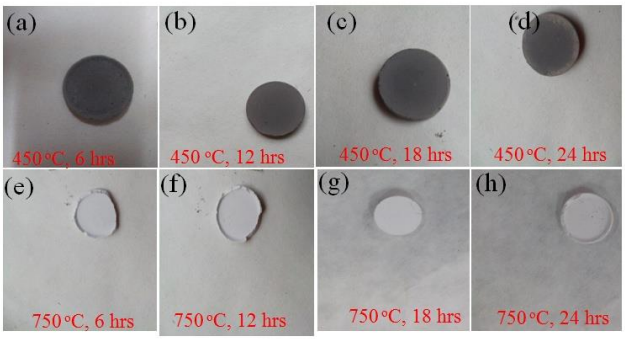

Fig. 1.Digital images of $Ca_2P_2O_7$ at (a) 120 ^{o}C for 12 hrs (b) 450 ^{o}C for 6 hrs (c) 450 ^{o}C for 12 hrs (d) 750 ^{o}C for 12 hrs.

3. Results and discussion

3.1. Colour changes

γ (Gamma) and β (beta) phases of $Ca_2P_2O_7$ pallets were obtained by solid state sintering for 6,12,18 and 24 hrs at 450 ^{o} C and 750 ^{o} C respectively. Gamma-$Ca_2P_2O_7$ grey colored phase is moderately hard while white colored β–$Ca_2P_2O_7$ is very brittle and soft. The optical micrographs of pellets annealed at 450 ^{o}C and 750 ^{o}C at different time intervals are shown in Fig. 1.

3.2 SEM analysis

Fig. 2 shows the SEM images of $Ca_2P_2O_7$ at (a) 450 ^{o}C for 6 hrs, (b) 450 ^{o}C for 12 hrs, (c) 450 ^{o}C for 18 hrs, (d) 450 ^{o}C for 24 hrs, (e) 750 ^{o}C for 6 hrs, (f) 750 ^{o}C for 12 hrs, (g) 750 ^{o}C for 18 hrs and (h) 750 ^{o}C for 24 hrs. The SEM images clearly show the cracks in both materials that were annealed at two different temperatures. These are due to thermal shocks as the samples were heated at a rate of 16^{o}C/min. It was critically noted that for a crack free surface, heating and cooling rate should not exceed 2 ^{o}C/min [10]. This behavior was also reported earlier in literature [10-12]. The SEM results show that the material particles were spherical and elongated in shape.

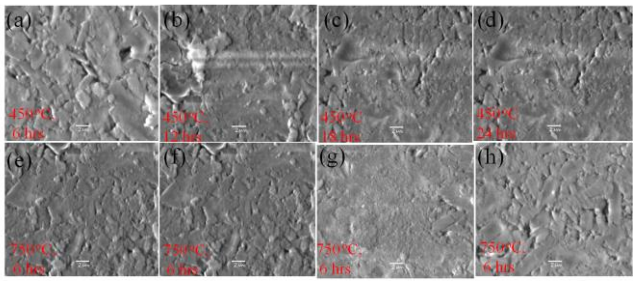

Fig. 2. SEM images of $Ca_2P_2O_7$ at (a) 120 °C for 12 hrs (b) 450 °C for 6 hrs (c) 450 °C for 12 hrs (d) 750 °C for 12 hrs.

3.3 XRD analysis

Fig. 3 shows the X-Ray Diffraction measurements of the samples sintered at 450 ◦C and 750 ◦C for 6,12,18 and 24hrs for XRD patterns at (a) 120 °C for 12 hrs (b) 450°C for 6 hrs (c) 450°C for 12 hrs (d) 750 °C for 12 hrs. The prominent XRD peaks for the tetragonal phase corresponding to for sharp reflections of $CaHPO_4$ at 2ϑ=28.985,30.435(211) (212) crystal plane respectively[13].The low intensity peaks for the phase at 2ϑ=40.57,41.87,54.08 corresponding to(098)(022) (203). Crystal planes were also observed at β- phase. XRD pattern of the samples sintered at 450 °C for 12 hrs showed relatively weak peaks at 2ϑ=11.5, 14, 20.817 corresponding to (221) (223) planes of gamma-phase of $CaHPO_4$ and relatively low peaks at 2ϑ=18.747, 26.348, 32.812, 36.910 corresponding to (112) (121) (212) (221). However XRD pattern revealed that the solid state reaction in this case was incomplete thus suggesting longer sintering time [7]. Critically noted that it is not the sintering temperature but the sintering time that is decisive in obtaining the phase transformation. Particle size of the starting material was also found to be an important parameter. Referring to the XRD patterns, sintering at 450 °C for 12 hrs shows sharp reflections of β-$CaHPO_4$ 2ϑ=26.677,27.597 for the planes of reflection (098) and (022) respectively [14]. However there are also low intensity peaks at 2ϑ= 41.85° ,43.29°, 50.43° to the tetragonal crystalline plane (121) (233) (322) respectively. The XRD pattern of the sample sintered at 450 °C showed the planes at 2ϑ: 26.67°(212), 27.59°(121), 30.76° (112), 34.80° (211). The medium intensity peaks occurring at 2ϑ=32.526°, 33.326° and 34.672° takes place around 450 °C and 750 °C. Transformation takes place around 450 °C and 750° C and above all temperature system remains in the phase till it melts at 1050 °C [8, 15].

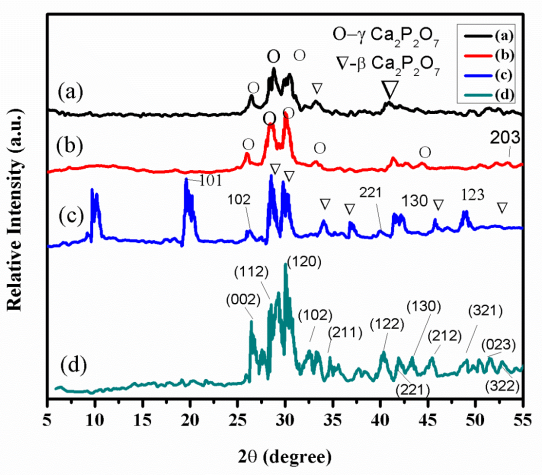

Fig. 3. XRD patterns of of $Ca_2P_2O_7$ at (a) 120 °C for 12 hrs (b) 450 °C for 6 hrs (c) 450 °C for 12 hrs (d) 750 °C for 12 hrs.

3.4 FTIR analysis

FTIR spectroscopy was utilized to characterize the different functional groups and metal-oxygen band positions. The FTIR spectra were recorded in the range of 4000-500 cm^{-1} at room temperature. FTIR spectra of both samples annealed at different temperature are shown in Fig. 4. These spectra exhibited the characteristic absorption peaks of materials annealed at 750 °C and 450 °C [16].The peaks in the range 937-1148cm^{-1} represented the PO_4 symmetric and asymmetric vibrations [17]. The peaks at 546-689 cm $^{-1}$ are due to the bending vibration of PO_4^{-3}. The intensity of these peaks in both samples were increased by calcinations temperature [18]. The asymmetric bending vibrations of samples were observed at 546, 651, 549, 592 cm^{-1}. The band at 774 cm^{-1} and 767 cm^{-1} are due to the symmetric stretching vibration of the bridged P-O bonds [9, 19].

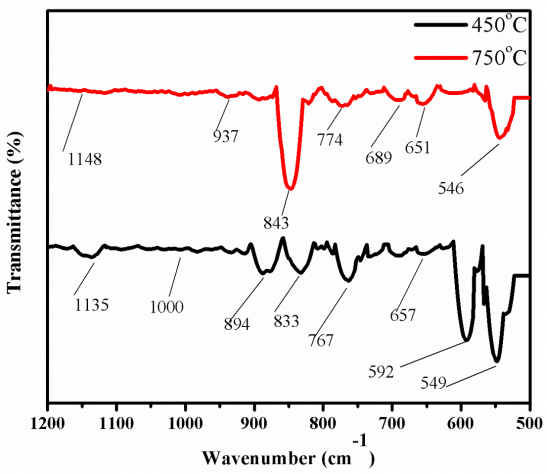

Fig. 4. FTIR spectrum of $Ca_2P_2O_7$ at 450 °C and 750 °C

3.5 TGA analysis

Thermal studies of samples were carried out by SDT Q600 V8.2 Build 100 thermal analyzer at temperature 10°C / min. TGA measurement showed the physical and chemical properties of materials as a function of temperature. Fig. 5 exhibit the TGA curve of $CaHPO_4$. TGA was carried out in the temperature range 50-700°C. Figure show that the weight loss was observed in two stages [16].The first weight loss was started at 50 °C because of the presence of water molecules in the sample material [20]. The second weight loss was observed at 640 °C because of the decomposition of $CaHPO_4$ to γ-$Ca_2P_2O_7$ [14]. After the second weight loss, the weight remained constant and further increase of temperature did not affect the weight of the material. [21].

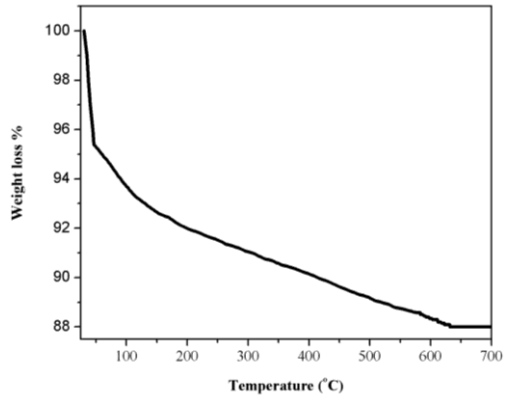

Fig. 5. TGA of $Ca_2P_2O_7$

3.6 UV-visible spectroscopic analysis

UV-Visible spectra were recorded on dual beam Agilent Cary 60 UV-Vis. Spectrometer. The range of wavelength was kept 200-800 nm. All the spectra were recorded at room temperature. The UV-Vis. Spectra are shown in Fig. 6. It is clear from the Figure that the γ-$Ca_2P_2O_7$ and β-$Ca_2P_2O_7$ both these materials exhibited the strong UV absorption at 240 nm. This band may be attributed to the π-π* transition [22]. These materials have potential applications in photocatalysis in the presence of UV light [23].

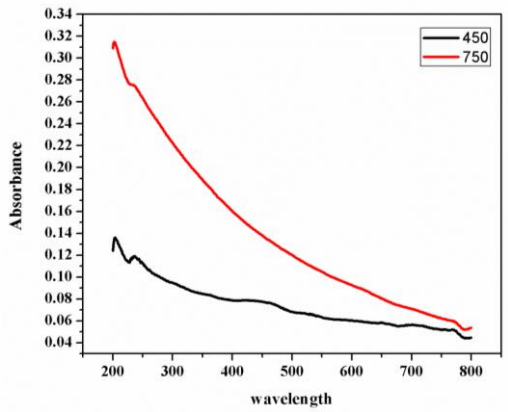

Fig. 6.UV-Vis spctrum of $Ca_2P_2O_7$ at 450 °C and 750 °C

3.7 Electric resistivity

Room temperature DC-electrical resistivity measurements of γ-$Ca_2P_2O_7$ and β-$Ca_2P_2O_7$ pellets were recorded by a two point probe method. The electric resistivity values from the obtained I-V data were determined using following relation [24].

$$\rho = R\frac{A}{L} \tag{2}$$

In above equation (2), the R is the resistance calculated from I-V curve, L is the thickness of the pellet and A is the cross-sectional area of the pellet. I-V curves are shown in the Fig. 7. Resistivity value of γ-$Ca_2P_2O_7$ and β-$Ca_2P_2O_7$ were found $\rho_{450} = 1.3\times10^9$ Ω-cm and $\rho_{750}=0.83\times10^9$ Ω-cm respectively [25]. It is clear from this data that the materials annealed at 450 °C are more resistive, while that the materials annealed at 750 °C is more conductive.

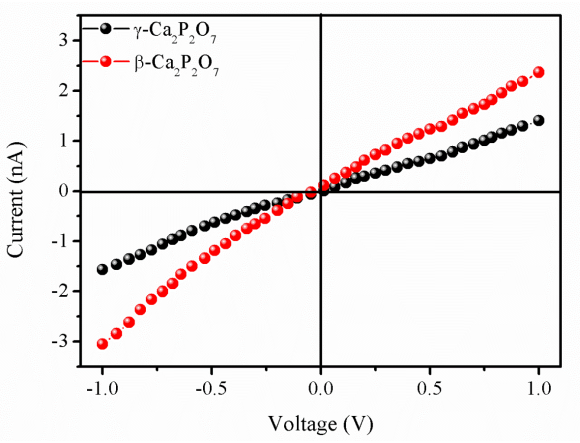

Fig. 7. I-V measurements of $Ca_2P_2O_7$ at 450 °C and 750 °C

4. Conclusion

The phase transformation could be obtained at 450 °C for gamma Phase and 750 °C for β phase. Scanning electron microscopy at 450 °C showed the more cracks as compared to the annealed at 750 °C. FTIR study confirmed the corresponding metal oxygen band positions. UV-Visble spectra showed the presence of absorption in UV range that may be exploited for photocatalysis applications in the presence of UV-radiations. Room temperature DC-resistivity measurements revealed that the β-$Ca_2P_2O_7$ is more resistive as compared to γ-$Ca_2P_2O_7$ phase. These materials have potential applications in photocatalysis, biomaterials and in medical physics.

Acknowledgement

The authors extend their sincere appreciations to the Deanship of Scientific Research at King Saud University

for its funding this Prolific Research Group (PRG-1436-26).

References

[1] H. Demirkiran, Y. Hu, L. Zuin, N. Appathurai, P. B. Aswath, Materials Science and Engineering: C, **31** 134 (2011).
[2] B. Boonchom, C. Danvirutai, Journal of Optoelectronics and Biomedical Materials **1,** 115 (2009).
[3] M. Lukić, Z. Stojanović, S. D. Škapin, M. Maček-Kržmanc, M. Mitrić, S. Marković, D. Uskoković, Journal of the European Ceramic Society **31**, 19 (2011).
[4] D. Veljović, I. Zalite, E. Palcevskis, I. Smiciklas, R. Petrović, D. Janaćković, Ceramics International **36**, 595 (2010).
[5] C. C. Silva, A. F. L. Almeida, R. S. de Oliveira, A.G. Pinheiro, J.C. Góes, A.S.B. Sombra, Journal of Materials Science **38,** 3713 (2003).
[6] S. Murakami, K. Kato, Y. Enari, M. Kamitakahara, N. Watanabe, K. Ioku, Ceramics International **38**, 1649 (2012).
[7] C. F. Koch, S. Johnson, D. Kumar, M. Jelinek, D. B. Chrisey, A. Doraiswamy, C. Jin, R. J. Narayan, I. N. Mihailescu, Materials Science and Engineering: C, **27**, 484 (2007).
[8] G. G. Chen, G. S. Luo, L. M. Yang, J. H. Xu, Y. Sun, J. D. Wang, Journal of Crystal Growth, **279**, 501 (2005).
[9] C. C. Silva, A. G. Pinheiro, M.A.R. Miranda, J.C. Góes, A. S. B. Sombra, Solid State Sciences, **5,** 553 (2003).
[10] M. Descamps, L. Boilet, G. Moreau, A. Tricoteaux, J. Lu, A. Leriche, V. Lardot, F. Cambier, Journal of the European Ceramic Society **33,** 1263 (2013).
[11] C. Nicolazo, H. Gautier, M.J. Brandao, G. Daculsi, C. Merle, Biomaterials **24**, 255 (2003).
[12] J. M. C. Q. Ning, A. El-ghannam, Journal of Materials Science **16**, 355 (2005).
[13] W.-F. Ho, H.-C. Hsu, S.-K. Hsu, C.-W. Hung, S.-C. Wu, Ceramics International **39,** 6467 (2013).
[14] D. Predoi, R. A. Vatasescu-balcan, R. T. I. Pasuk, M. Costache, J. Optoelectron. Adv. Mater. **10**, 5678 (2008).
[15] A. C. Tas, Journal of the European Ceramic Society **20,** 2389 (2000).
[16] S. Mondal, B. Mondal, A. Dey, S. Mukhopadhyay, Journal of Minerals and Materials Characterization and Engineering **11**, 55 (2012).
[17] S. Shanmugam, B. Gopal, Ceramics International **40**, 15655 (2014).
[18] D. K. Pattanayak, D. P. S. Upadhyay, R. C. Prasad, B. T. Rao, T. R. R. Mohan, Trends Biomater. Artif. Organs **18**, 87 (2005).
[19] S. Mandel, A. C. Tas, Materials Science and Engineering: C, **30,** 245 (2010).
[20] K. C. B. Yeong, J. Wang, S. C. Ng, Biomaterials **22**, 2705 (2001).
[21] T. V. Safronova, V. I. Putlayev, K. A. Bessonov, V. K. Ivanov, Processing and Application of Ceramics **7,** 9 (2014).
[22] X. Teng, M. Yan, H. Bi, Spectrochimica Acta Part A: Molecular and Biomolecular Spectroscopy **118,** 1020 (2014).
[23] K. Krishnamoorthy, G.-S. Kim, S. J. Kim, Ultrasonics Sonochemistry **20,** 644 (2013).
[24] M. B. Runge, M. Dadsetan, J. Baltrusaitis, M. J. Yaszemski, Journal of biological regulators and homeostatic agents **25,** S15 (2011).
[25] G. H. Cai, Y. J. Du, S. Y. Liu, D. N. Singh, Canadian Geotechnical Journal, **1,** 678 (2015).

*Corresponding author: kimtiaz1122@yahoo.com